

TS-1 from first principles.

Journal:	<i>The Journal of Physical Chemistry</i>
Manuscript ID:	jp-2009-05110s.R1
Manuscript Type:	Special Issue Article
Date Submitted by the Author:	22-Jul-2009
Complete List of Authors:	Gamba, Aldo; Ambientali - CO, Dipartimento di Scienze Chimiche E Tabacchi, Gloria; Universita' dell'Insubria, Dipartimento di Scienze Chimiche ed Ambientali Fois, Ettore; Universita' Insubria, Dipartimento Scienze Chimiche e Ambientali

SCHOLARONE™
Manuscripts

TS-1 from first principles.

Aldo Gamba*, Gloria Tabacchi and Ettore Fois

July 22, 2009

Dipartimento di Scienze Chimiche ed Ambientali, University of Insubria, and INSTM,
Via Lucini 3, I-22100 Como (Italy)

Abstract

First principles studies on periodic TS-1 models at Ti content corresponding to 1.35% and 2.7% in weight of TiO_2 are presented. The problem of Ti preferential siting is addressed by using realistic models corresponding to the TS-1 unit cell $[\text{TiSi}_{95}\text{O}_{192}]$ and adopting for the first time a periodic DFT approach, thus providing an energy scale for Ti in the different crystallographic sites in non defective TS-1. The structure with Ti in site T3 is the most stable, followed by T4 (+0.3 kcal/mol), while the less stable structure, corresponding to Ti in T1, is 5.6 kcal/mol higher in energy. The work has been extended to investigate models with two Ti per unit cell $[\text{Ti}_2\text{Si}_{94}\text{O}_{192}]$ (2.7%). The possible existence of Ti-O-Ti bridges, formed by two corner sharing TiO_4 tetrahedra, is discussed. By using cluster models cut from the optimized periodic DFT structures, both vibrational (DFT) and electronic excitation spectra (TDDFT) have been calculated and favourably compared with the experimental data available on TS-1. Interesting features emerged from excitation spectra: i) isolated tetrahedral Ti sites show a Beer-Lambert behavior, with absorption intensity proportional to concentration. Such a behaviour is gradually lost when two Ti occupy sites close to each other; ii) the UV-Vis absorption in the 200-250 nm region can be associated to transitions from occupied states delocalized on the framework oxygens to empty d states localized on Ti. Such extended states-to-local states transitions may help the interpretation of the photovoltaic activity recently detected in Ti zeolites.

Part of the "Vincenzo Aquilanti Festschrift"

1 Introduction

TS-1, titanium silicalite, is a porous crystalline material broadly used in industrial plants as a catalyst for hydrocarbons oxidative processes.¹ Since it allows to operate

1
2
3
4
5 at mild conditions using hydrogen peroxide as oxygen source and generating water as
6 a by-product, its discovery² is considered a milestone in the development of modern
7 heterogeneous catalysts for sustainable technologies. For this reason, TS-1 has been
8 one of the most extensively studied zeolitic materials and much attention is still fo-
9 cused on its unique physico-chemical and reactivity properties. Besides its relevance
10 in catalysis, TS-1 is currently of interest for advanced applications in other fields, such
11 as solar cell technology. Indeed, titanium zeolites have recently been shown to exhibit
12 photovoltaic activity,³ thus suggesting their use in dye-sensitized solar cells as porous
13 electron-transport materials as an alternative to dense TiO₂ nanoparticles.

23 From the structural point of view, TS-1 is a zeolite with MFI framework topology.⁴
24 The all-silica phase of MFI, the catalytically inactive Silicalite-1, has a unit cell con-
25 tent corresponding to [Si₉₆O₁₉₂]. The as-synthesized Silicalite-1, containing tetrapropy-
26 lammonium cation (TPA⁺) as structure directing agent (SDA), has an orthorhombic
27 structure.⁵ The calcined form of Silicalite-1 has a monoclinic unit cell with $\alpha=90.6^\circ$
28 (see e.g. Ref.⁶). The catalytically active phase TS-1, which is characterized by a low
29 Ti content (below 3.0% in weight of TiO₂), is orthorhombic.⁶ It can be considered a
30 solid solution of TiO₂ in zeolitic SiO₂, where only a small portion of tetrahedral sites
31 (T sites) are isomorphously occupied by Ti. Thus in TS-1, and in general, in tita-
32 nium zeolites, Ti is surrounded by 4 oxygen atoms in a tetrahedral environment and is
33 therefore undercoordinated with respect to the stable TiO₂ phases, where Ti occupies
34 octahedral sites (TiO₆). Indeed, it is believed that such a Ti fourfold coordination is
35 the actual responsible of Ti zeolites catalytic activity, because TiO₂ contents higher
36 than 3% lead to phase separation of octahedral TiO₂ phases and deactivation of the
37 catalytic properties of the material.⁷

54 In view of its role in industrial catalysis, TS-1 has been the subject of many experimen-
55 tal investigations carried out with a variety of spectroscopic techniques. In spite of the
56 broad benchmark of UV-Vis, IR, raman, and X-ray data on Ti sites in TS-1 available in
57
58
59
60

1
2
3
4
5 the literature,⁸⁻¹¹ details of the TS-1 structure at the microscopic level are still unclear.
6
7 One of such issues is concerned with the Ti location in TS-1. Diffraction studies¹²⁻¹⁴
8
9 suggested a nonrandom distribution of Ti in the tetrahedral T sites of TS-1. However,
10
11 there is still no general consensus on the T sites actually occupied by Ti in TS-1, and
12
13 different siting probabilities were reported (see ref.¹⁵).
14

15
16 The uncertainty in locating Ti is associated with the low Ti concentration, correspond-
17
18 ing to approximately 2-3 Ti atoms in the TS-1 unit cell. Moreover, due to its large unit
19
20 cell size and low Ti content ($[\text{Ti}_x\text{Si}_{96-x}\text{O}_{192}]$), this crystalline catalyst has escaped a
21
22 thorough theoretical characterization to date. Studies aimed at establishing the loca-
23
24 tion of Ti in TS-1 have been performed only by adopting force-field based schemes^{16,17}
25
26 or quantum mechanical methods on cluster or embedded cluster models (see e.g.^{15,18}).
27
28 Primary goal of this work is to fill this gap, by performing a series of Density Func-
29
30 tional Theory (DFT) calculations by using for the first time a first-principles periodic
31
32 approach for such a large system.
33

34
35 Although the high calcination temperature needed to obtain the active TS-1 catalyst
36
37 may suggest a role of thermodynamics in ruling the Ti distribution in the different
38
39 T sites, the microscopic origin of Ti preferential siting is still a matter of discussion,
40
41 and a series of hypotheses have been formulated (see e.g. Ref.^{12,15,19}). It has been
42
43 proposed that kinetic factors may be the predominant ones in determining the actual
44
45 Ti location.¹⁵ Also, it has been suggested that, already during the nucleation and
46
47 growth process, Ti siting may be influenced by the distribution of the structure direct-
48
49 ing agent, because of the coulomb interactions between positively charged SDAs and
50
51 pentavalent anionic (hydroxylated) Ti centers detected in as-synthesized (non calcined)
52
53 TS-1.¹⁹ Moreover, it has been reported that the disappearance of defect centers (e.g.
54
55 Si-OH groups) correlates with an increase of Ti concentration, suggesting the idea that
56
57 Ti replaces defective sites in TS-1.¹² In this scenario, our work is aimed at establishing
58
59 an energy scale for Ti occupancy in the different tetrahedral sites of TS-1 by using a
60

1
2
3
4
5 periodic DFT approach.
6

7 Since in the orthorhombic MFI framework there are 12 crystallographically different
8 tetrahedral sites, geometry optimizations have been carried out on 12 [TiSi₉₅O₁₉₂]
9 structures obtained by placing Ti in one of the twelve inequivalent T positions. These
10 structures correspond to a title of 1.35% in weight of TiO₂. Optimizations have been
11 also performed on structures characterized by a [Ti₂Si₉₄O₁₉₂] stoichiometry, in order
12 to explore the energetics of TS-1 models at a 2.7% Ti content. In this case, a system-
13 atic computational investigation is prevented by the number of possible structures: as
14 there are 12 T sites, each with multiplicity 8, there are $96!/(2!(96-2)!)=4608$ possible
15 structures characterized by different location of 2 Ti atoms. However, relevant insight
16 has been gathered by focusing the analysis on a restricted subset of models, thus en-
17 abling to quantify the energy separation among the different Ti distributions for a TS-1
18 framework characterized by a Ti content close to that typical of the actual catalytic
19 material.
20
21
22
23
24
25
26
27
28
29
30
31
32

33 Besides energetic issues related to Ti siting, electronic and vibrational properties of Ti
34 in the different tetrahedral sites of the TS-1 model systems were studied. A thorough
35 analysis has been performed on electronic excitation spectra in the UV-Vis region,
36 where a signature of zeolitic titanium is detected at around 200-250 nm.²⁰ Moreover,
37 IR and raman spectra were calculated and compared with the corresponding spectro-
38 scopic data,^{8,9} which also exhibit fingerprints of framework Ti. From such a theoretical
39 characterization of Ti sites, combined with the analysis of their energy stability, reliable
40 predictions about the Ti distribution in TS-1 could be deduced.
41
42
43
44
45
46
47
48
49
50

51 **2 Methods of calculations and Models**

52
53
54

55 The orthorhombic framework of TS-1 (space group Pmna, see e.g. Ref.¹²) is character-
56 ized by interconnected channels, whose section is formed by 10-membered rings. The
57 secondary building unit is a 5-1 structure characterized by a 5-membered ring (5-ring).⁴
58
59
60

1
2
3
4
5 There are 12 non equivalent T sites (each with multiplicity 8) and 26 non equivalent
6 O sites (see Figure 1). The twelve possible structures [TiSi₉₅O₁₉₂], identifiable by the
7 location of Ti in one of the 12 sites (labelled T1, T2, T3, ..., T12), were studied by
8 adopting plane waves as basis set and the PBE gradient corrected DFT functional.²¹
9
10 The geometry of each of the 12 [TiSi₉₅O₁₉₂] systems (T1,T2,..T12 from now on) was
11 optimized by using ultra soft Vanderbilt pseudopotentials²² with a 30 Ry cutoff for the
12 plane waves expansion of the orbitals, and a 180 Ry cutoff for the electronic density
13 (PBE/VDB/30) at the Γ point. Periodic boundary conditions were applied.
14
15
16
17
18
19
20
21

22 Such a computational scheme, based on ultra-soft pseudopotentials and PBE approx-
23 imation to DFT, has been successfully adopted in the study of the structure and the
24 energetics of large systems, like e.g. TiO₂ surfaces²³ and aluminosilicate porous ma-
25 terials.²⁴ Moreover, the PBE approximation has proven reliable for the structure and
26 energetics of other heteroatom substituted zeolite structures, like boron zeolites.^{25,26}
27
28
29
30
31

32 Optimizations were carried out, using a quasi-Newton scheme, at fixed cell pa-
33 rameters (fixed volume), while no constraint was imposed on the nuclear positions.
34 Optimizations were considered converged when the maximum force on atoms was less
35 than 10⁻⁴ a.u.. The CPMD code²⁷ was used for the plane waves periodic DFT cal-
36 culations. The cell parameters adopted in the calculations (a=20.049 Å, b=19.926 Å,
37 c=13.401 Å), are extracted from diffraction studies on TS-1 with corresponding Ti
38 content.¹² With the same computational setup, we have optimized the structures of
39 few [Ti₂Si₉₄O₁₉₂] models, obtained by placing Ti in two T sites, and adopting cell pa-
40 rameters (a=20.113 Å, b=19.930 Å, and c=13.410 Å) corresponding to a TS-1 sample
41 of comparable Ti content.¹²
42
43
44
45
46
47
48
49
50
51

52 For the electronic excitation spectra calculations, two different approaches were adopted.
53 In one, the cluster approach, time dependent DFT (TD-DFT)^{28,29} calculations were
54 carried out on Ti containing clusters cut from the PBE/VDB/30 optimized periodic
55 structures. Three cluster models of different size were adopted, namely C_{tetra} , C_{5-ring}
56
57
58
59
60

1
2
3
4
5 and C_{2tetra} , represented in Figure 1. In the smallest model C_{tetra} , with stoichiometry
6 $Ti-[O-(Si(OH)_3)_4]$, Ti is surrounded by four tetrahedral building units, i.e., by two
7 oxygen atoms shells. Oxygens in the second shell were saturated with H atoms lo-
8 cated at 1.0 Å from O, along the O-Si bond direction in the corresponding optimized
9 crystal structure. Cluster C_{5-ring} contains a 5-ring structure and is characterized by
10 a $Ti_xSi_{9-x}O_9(OH)_{18}$ stoichiometry, while C_{2tetra} is formed by two corner sharing C_{tetra}
11 clusters and has a $Ti_xSi_{8-x}O_7(OH)_{18}$ formula. Systems with $x=0,1,2$ have been con-
12 sidered. The C_{5-ring} and the C_{2tetra} clusters were used, with $x=2$, to investigate the
13 properties of Ti-O-Si-O-Ti and Ti-O-Ti bridges respectively. The external oxygen
14 atoms were saturated by the same procedure adopted in the C_{tetra} model. TD-DFT
15 excitations were calculated using the hybrid B3LYP functional³⁰ and a gaussian basis
16 set (6-311+g**).³¹ Convergence was required for at least 50 excited states. We shall
17 refer to these results as TDDFT/Cluster.

18
19 In a second approach, the electronic excitation spectrum was calculated by adopting pe-
20 riodic boundary conditions. Specifically, the optical conductivity of the PBE/VDB/30
21 optimized structures was calculated by using the PBE functional and norm conserv-
22 ing pseudopotentials^{32,33} with a cutoff of 110 Ry for the plane wave expansion of the
23 orbitals and 440 Ry for the electronic density. In the case of large periodic systems,
24 the more accurate TD-DFT approach for electronic excitations is not viable, however,
25 gradient corrected DFT gives results quite close to TD-DFT in the case of Ti-zeolite
26 systems.³⁴⁻³⁶ We shall refer to these calculations as DFT/pbc.

27
28 In the calculated electronic excitation spectra, both DFT/pbc and TDDFT/cluster, a
29 line broadening of 2.0 nm was applied.

30
31 Vibrational properties, IR and raman, were calculated on the above described cluster
32 models. To this aim, the clusters geometries have been re-optimized using the B3LYP
33 functional and the 6-311g** basis set. In the minimization process, the "external"
34 O-H atoms were kept fixed in order to mimic the constraint due to the full crystal
35
36
37
38
39
40
41
42
43
44
45
46
47
48
49
50
51
52
53
54
55
56
57
58
59
60

1
2
3
4
5 and to decouple the calculated vibrational spectra from signals due to modes involving
6
7 O-H groups. Such modes are known to interfere in the silica window, an otherwise
8
9 transparent region between 850-1000 cm^{-1} typical of SiO_2 materials, where signals of
10
11 tetrahedral Ti can be found. All the spectra are calculated within the harmonic ap-
12
13 proximation and obtained from stationary points, characterized by positive frequencies.
14
15 A line broadening of 10 cm^{-1} was used for both IR and raman spectra representations.
16
17 As common practice in comparing with experimental data, a shift factor of 0.98 was
18
19 applied to the calculated wavenumbers.³⁷
20
21
22
23
24

25 **3 Results**

26 **3.1 Structure and Energetics**

27
28
29
30 The minimum energy structure among the twelve $[\text{TiSi}_{95}\text{O}_{192}]$ models corresponds to
31
32 the one where Ti occupies site T3. Such a structure is however only 0.28 kcal/mol
33
34 below the one with Ti in T4, while the highest energy structure, 5.6 kcal/mol above
35
36 the T3, corresponds to Ti in T1. Therefore it turns out that energy differences among
37
38 TS-1 systems characterized by 1.35% Ti are within 5.6 kcal/mol. Remarkably, nine
39
40 out of twelve structures are in the 4 kcal/mol range from the minimum.
41

42
43 The calculated Ti-O bond distances and O-Ti-O bond angles are reported in Table
44
45 1 and Table 2, respectively. It should be said at the outset that all Ti sites have a
46
47 slightly distorted tetrahedral structure. In general, the calculated Ti-O bond lengths
48
49 are in agreement with the value of 1.793 Å reported from in vacuo X-ray spectroscopies
50
51 studies on calcinated TS-1 samples.¹¹ The trends of: i) average Ti-O bond distances,
52
53 ii) Ti-Si (first-neighbors) distances and iii) Ti-O-Si angles as a function of Ti siting
54
55 in the twelve $[\text{TiSi}_{95}\text{O}_{192}]$ optimized structures are reported in Figure 2 along with
56
57 the energy differences ΔE . Also reported in Figure 2 are the (normalized) probability
58
59 associated to Ti occupancy of the different T sites. Probabilities were calculated, from
60

1
2
3
4
5 the Boltzmann factor $\exp(-\Delta E/kT)$, for room temperature and for 500°C, a commonly
6 adopted calcination temperature. It can be deduced, on purely energetics grounds, that
7 the T3 and T4 sites would account for more than 50% of Ti even at high calcination
8 temperatures.
9

10
11 Selected configurations with stoichiometry $[\text{Ti}_2\text{Si}_{94}\text{O}_{192}]$, corresponding to two Ti per
12 unit cell, have been optimized as well. They represent only a subset of the many
13 possible configurations with such a Ti content. In all cases one Ti (Ti^1) was placed in
14 one T3 site, corresponding to the minimum energy monosubstituted structure, while
15 the location of second Ti (Ti^2) varied, and a total of twenty different configurations
16 were optimized. The Ti^1 - Ti^2 pairs, their Ti-Ti distances and the relative stability
17 are graphically represented in Figure 3. The most stable system corresponds to a
18 configuration with Ti^2 in a T4 site at about 7.3 Å from Ti^1 . However most of the
19 optimized structures are within 6 kcal/mol from the minimum energy arrangement. It
20 is to notice that the energy difference depends not only on the pair of sites but also on
21 their actual separation. On the other hand, in the case of Ti in T3-T5 two T5 sites
22 are available at similar distances from T3 (at about 5.2 Å), but the two corresponding
23 arrangements differ by 1.3 kcal/mol. This finding indicates that also the details of the
24 Ti centres local environment may affect the relative stability of systems characterized
25 by different Ti distributions.
26
27

28
29 Two systems containing adjacent T sites, characterized by a Ti-O-Ti bridge and a Ti-Ti
30 distance of ~ 3.5 Å, were also considered: the first one, and most stable of the two, with
31 the second Ti (Ti^2) in T4 and the second structure with Ti^2 in T6. The two structures
32 differ by 4.3 kcal/mol; therefore, also for systems with corner sharing TO_4 , the relative
33 energy depends on the pair of T sites actually occupied by Ti. Remarkably, the T3-T4
34 Ti-O-Ti bridge structure is only 2.7 kcal/mol higher than the most stable system with
35 the same Ti content. Its Ti-O bond distances and O-Ti-O angles, reported in Tables
36 3 and 4 respectively, are very close to the ones calculated for the systems containing a
37
38
39
40
41
42
43
44
45
46
47
48
49
50
51
52
53
54
55
56
57
58
59
60

1
2
3
4
5 single Ti site. This indicates that the formation of a Ti-O-Ti bridge implies only small
6 distortions in the geometry of the TiO_4 units. Moreover, the Ti-O-Ti bonds forming
7 the bridge are the shortest ones among the systems here considered.
8
9

10 11 **3.2 Vibrational analysis**

12
13
14
15 IR and raman spectra have been of overwhelming relevance in unravelling the structure
16 of the Ti sites in TS-1 and related materials (see e.g. ref.^{8,9}). An IR feature at 960 cm^{-1}
17 has been associated with Ti in zeolitic tetrahedral sites. Moreover, the intensity of such
18 a band has been proved to be related to the content of tetrahedral Ti in TS-1.³⁸ Also,
19 a raman signature at 1125 cm^{-1} has been associated to tetrahedral Ti. In Figure 4a
20 the calculated IR and raman predictions are shown for a Ti containing cluster and for
21 the equivalent all-silica one. The spectrum of the T3 centered C_{tetra} system is reported
22 in Figure 4a, along with that calculated for a C_{5-ring} with one Ti in T3. As clusters
23 centered on different crystallographic T sites have very similar vibrational properties,
24 only the T3 case will be discussed. In the small C_{tetra} cluster, a peak at about 980
25 cm^{-1} (with a shoulder at 1005 cm^{-1}) is associated with the presence of Ti, both in the
26 IR and in the raman predictions. In the larger C_{5-ring} system, the 980 cm^{-1} feature
27 is red-shifted to 958 cm^{-1} . In the raman activity spectrum, the small C_{tetra} cluster
28 shows an intense peak at 1128 cm^{-1} , which is shifted to 1135 cm^{-1} in C_{5-ring} . In both
29 cases, such a raman active mode is related to an in-phase (symmetric) stretching of
30 the TiO_4 unit. It is to point out that the above discussed features are missing in the
31 spectra of an all silica C_{5-ring} cluster reported in Figure 4a for comparison, and should
32 therefore be attributed to the presence of tetrahedral Ti. Remarkably, both IR and
33 raman results are in line with experimental findings.^{8,9}
34
35
36
37
38
39
40
41
42
43
44
45
46
47
48
49
50
51
52
53

54 In Figure 4b and 4c, the vibrational spectra calculated for clusters containing two
55 close Ti atoms are shown, one is relative a Ti-O-Ti bridge, the other to a Ti-O-Si-O-Ti
56 structure respectively. Let us discuss the vibrational properties of a C_{2tetra} system
57 containing a Ti-O-Ti bridge (Figure 4b). In the IR spectrum, such a system is char-
58
59
60

acterized by two Ti-related features, at 853 cm^{-1} and at 1006 cm^{-1} , both located at the edges of the silica window. A very intense raman-active peak is found at 1114 cm^{-1} , two weaker raman signals are found at 978 and 1003 cm^{-1} . Also a very weak raman signal is calculated at 853 cm^{-1} . The above IR and raman signals are due to the Ti-O-Ti bridge, as they are missing in the spectra of the other C_{2tetra} clusters, reported in Figure 4b, which do not contain such a bridge.

In the case of a C_{5-ring} characterized by a Ti-O-Si-O-Ti bridge (Figure 4c), the IR signal at 958 cm^{-1} typical of an isolated tetrahedral Ti is enhanced in intensity, however a new feature appears at 908 cm^{-1} . In the raman spectrum, the 1135 cm^{-1} signal typical of isolated Ti is splitted and red-shifted at 1110 cm^{-1} . The 958 cm^{-1} raman feature is red-shifted to 908 cm^{-1} in passing from a C_{5-ring} with only one Ti to a C_{5-ring} with a Ti-O-Si-O-Ti bridge. The above discussed features are absent (both IR and raman) in the all-silica C_{5-ring} system spectra reported in Figure 4c for comparison.

3.3 Electronic excitation spectra

UV-Vis spectra of dry TS-1 and other Ti-zeolites are characterized by a broad absorption band at 200-250 nm,^{9,20,39} which is considered the fingerprint of tetraordinated Ti in the zeolite framework. Band profiles, as well as maximum position and intensity, slightly vary among the wealth of available experimental data: for instance, a 208-210 nm peak position is reported for dry TS-1,^{11,40} while other studies on the same system reported, after deconvolution, a strong peak at 199 nm and two weaker bands at 226 and 248 nm respectively.¹⁰ However, a general agreement exists in interpreting these bands as ligand to metal charge transfer (LMCT) transitions from occupied oxygen states to empty Ti d orbitals in tetrahedral TiO_4 units.

Combination of periodic DFT calculations with the TDDFT/cluster approach provides a reliable theoretical description of electronic properties of zeolitic Ti.³⁵ Unless otherwise stated, the results here presented refer to TD-DFT excitations calculated for clusters extracted from optimized PBE/VDB/30 models.

1
2
3
4
5 The electronic excitation spectra calculated for the 12 Ti-centered C_{tetra} clusters, re-
6 ported in Figures 5-6, show absorptions in the 200-230 nm region typical of experi-
7 mental spectra of Ti-zeolites. In order to exclude that calculated excitations derive
8 from artifacts of the adopted approximations, the electronic spectrum of a T1 cluster
9 extracted from silicalite was calculated as well. By comparing the Ti- and Si- centered
10 systems (Figure 5) it clearly emerges that the 200-230 nm band is due to tetrahedral
11 TiO_4 , in line with the current interpretation, and with previous theoretical studies.^{35,36}
12 Moreover, calculations for Ti in the T6 site performed on both C_{tetra} and C_{5-ring} clus-
13 ters provided analogous electronic structure descriptions and very close wavenumbers
14 for the lowest energy transition ($\Delta\lambda_{max} = 1.1$ nm). Therefore, the results presented
15 below are not significantly affected by cluster size effects.
16
17
18
19
20
21
22
23
24
25
26
27

28 Calculated electronic excitation spectra show different profiles but are all charac-
29 terized by multiple peaks. The presence of multiple bands derives, in general, from the
30 splitting of the empty Ti 3d and of the occupied O 2p states as a consequence of the
31 quasi-tetrahedral T-site environment, as highlighted by previous work on different Ti-
32 zeolites.³⁶ By a thorough analysis of the electronic structure in terms of the molecular
33 orbitals involved in the excitations, a detailed description of the electronic transitions
34 that characterize Ti in the 12 different T sites can be obtained.
35
36
37
38
39
40
41

42 In the C_{tetra} (Ti-[O-(Si(OH)₃]₄) clusters, the lower energy empty molecular orbitals
43 (MO) are mostly localized on Ti and may be described in terms of crystal field theory
44 (CFT) in the case of tetrahedral coordination. More specifically, the two lowest empty
45 MOs, the LUMO and LUMO+1, may be correlated with the Ti d_{z^2} and Ti $d_{x^2-y^2}$
46 states, while the MOs from LUMO+2 to LUMO+7 are due to combinations of Ti
47 d_{xy} , d_{xz} , d_{yz} with framework oxygens lone pairs (Figure 7). By borrowing the familiar
48 CFT notation, we shall refer to these two groups of states as $e_g^{(E)}$ and $t_{2g}^{(E)}$ respectively,
49 where (E) stays for "empty". However, at difference with the case of an ideal tetra-
50 hedron, here degeneracy of the $e_g^{(E)}$ and of the $t_{2g}^{(E)}$ states is removed because TS-1
51
52
53
54
55
56
57
58
59
60

1
2
3
4
5 actually provides distorted tetrahedral environments to the metal center. In addition,
6
7 such distortions are different for each T site, and depend not only on the local TiO_4
8
9 geometry, but are also related to Ti-Si separations, Ti-O-Si angles and, in general, to
10
11 the arrangement of the SiO_4 units around Ti. This leads to slightly different orbital
12
13 splitting patterns among the 12 model systems; in particular, $e_g^{(E)}$ and $t_{2g}^{(E)}$ states are
14
15 separated by energy differences ranging from 0.58 eV (T10) to 0.95 eV (T8), while the
16
17 LUMO-LUMO+1 separation ($e_g^{(E)}$ splitting) varies between 0.045 eV (T4) and 0.174
18
19 eV (T6).
20

21
22 As a first approximation, a CFT-like description could be adopted also for the 32 higher
23
24 energy occupied states of the C_{tetra} models, where the dominant contribution comes
25
26 from the O 2p lone pairs (two for each of the 16 O atoms). In tetrahedral symmetry,
27
28 they are split in three groups, that could be labelled $t_{2g}^{(O)}$, $t_{2g}^{(O-1)}$ and $e_g^{(O)}$ in decreasing
29
30 energy order (with O indicating “occupied”). These MOs contain however non negli-
31
32 gible contributions of the Ti d orbitals. Thus, besides the details of T site geometry
33
34 and symmetry, their energy ladder also depends on the extent of contamination with
35
36 metal states. Actually, the details of the electronic structure in the frontier MOs region
37
38 change among the 12 T site models and such variations are not straightforwardly re-
39
40 lated to simple structural parameters such as Ti-O bond distances. These observations
41
42 explain why the calculated spectra differ in the number, position, and intensity of the
43
44 peaks and, at the same time, suggest that determining Ti-siting simply from analysis of
45
46 UV-Vis band profiles could be a very difficult task, even in the case of a non-defective
47
48 TS-1. Indeed, optical spectra of systems characterized by different Ti locations share
49
50 a number of common features, as detailed below.
51

52
53 A graphical representation of relevant orbitals is shown in Figure 7 for the case of Ti
54
55 in T6. The occupied MOs involved in electronic transitions are the $t_{2g}^{(O)}$ ones. In the
56
57 C_{tetra} clusters, they correspond to the 12 states from HOMO to HOMO-11, and may
58
59 be grouped into two subsets. While the higher energy $t_{2g}^{(O)}$ states are basically non-
60

1
2
3
4
5 bonding O 2p combinations ($nb-t_{2g}^{(O)}$), the ones at lower energy are characterized by
6 mixing with Ti d states and present therefore a certain degree of Ti-O bonding char-
7 acter ($b-t_{2g}^{(O)}$). Moreover, the frontier occupied MOs are not strictly localized on the
8 Ti-bound oxygens, but should formally be regarded as extended over all the oxygens
9 in the model system. Such an electronic structure description holds for larger C_{5-ring}
10 models as well, as clearly shown in Figure 8. In particular, while the HOMO is mainly
11 localized on the Ti-bound oxygens, other $nb-t_{2g}^{(O)}$ are delocalized over the whole 5-ring
12 system. Therefore, by extrapolating to the solid, LMCT electronic transitions in low
13 Ti-content TS-1 essentially go from the $t_{2g}^{(O)}$ band to the localized Ti d states.
14
15

16 The edge (lowest energy absorption) of the calculated spectra, ranging from 223.2 (T1)
17 and 230.7 (T6) nm, is mainly due to the HOMO→LUMO transition, with however
18 significant contributions from the HOMO-1→LUMO and HOMO-2→LUMO excita-
19 tions. The higher wavelength peak (210-225 nm) is due to $nb-t_{2g}^{(O)} \rightarrow e_g^{(E)}$ transitions
20 and has a pure LMCT character, while bands between 195 and 210 nm derive from
21 $b-t_{2g}^{(O)} \rightarrow e_g^{(E)}$ transitions and might be considered LMCT contaminated by O 2p - Ti
22 d mixing. Interestingly, the $t_{2g}^{(E)}$ states do not contribute to the bands above 200 nm
23 because of their quite large energy separation from the $e_g^{(E)}$ ones. Indeed, absorptions
24 below 190 nm are mainly related to lower intensity $t_{2g}^{(O)} \rightarrow t_{2g}^{(E)}$ transitions; however, in
25 the real material, such bands should be at least partially obscured by the silica matrix
26 absorptions.
27
28

29 Let us now consider the excitation spectra for the higher Ti-content TS-1 systems
30 (Figures 9-11). It should be stressed at the outset that, also in this case, DFT/pbc and
31 TDDFT/cluster approaches provide very close representations of electronic excitation
32 properties, leading to similar band profiles and peak position differences in the 10 nm
33 range (Figures 10-11).
34
35

36 Electronic spectra were calculated for models characterized by different arrangements
37 of the two Ti atoms in the TS-1 cell. In particular, T site locations and Ti^1-Ti^2
38
39
40
41
42
43
44
45
46
47
48
49
50
51
52
53
54
55
56
57
58
59
60

1
2
3
4
5
6 separations were selected with the aim of discriminating, in the calculated spectra, the
7 effect of the Ti content increase (Figure 9) from that of the Ti-Ti interaction (Figures
8 10-11).
9

10
11 The effect of Ti content on TS-1 electronic spectra is clearly pictured in Figure 9.
12 Here, a $[\text{Ti}_2\text{Si}_{94}\text{O}_{192}]$ model with two Ti atoms located in two T3 sites separated by
13 14 Å has been considered and electronic excitations calculated with the DFT/ptc
14 approach. Remarkably, the optical conductivity of this system amounts to twice the
15 one calculated for $[\text{TiSi}_{95}\text{O}_{192}]$ with Ti in T3. On these basis, it could be predicted
16 that UV-Vis spectra of TS-1 systems with well separated (non-interacting) Ti centers
17 will be characterized by an intensity proportional to the Ti content, i.e. following the
18 Beer-Lambert law. Closer Ti centers should lead to deviations from the Beer-Lambert
19 behaviour. Such a prediction is confirmed by comparing electronic spectra of systems
20 containing two close Ti atoms with those of the corresponding low-Ti content models.
21 In the case of a representative Ti-O-Si-O-Ti structure, where Ti^1 is in T3, Ti^2 in T6
22 and the Ti^1 - Ti^2 separation amounts to 5.605 Å, a Beer-Lambert like behaviour is still
23 observed: intensities are approximately additive and only a small red-shift of the edge
24 is detected (see Figure 10). Indeed, analysis of the TD-DFT excitations and of the
25 MOs involved in the transitions indicates that the presence of two non-adjacent Ti
26 centers perturbs but does not alter substantially the electronic structure of the TS-1
27 system with respect to the case of “isolated” (or well-separated) Ti centers. Therefore,
28 the optical spectrum of a system with two TiO_4 units interconnected by a Si in close
29 T sites could approximately be described as the sum of two spectra, each related
30 to isolated TiO_4 in one of the sites (namely, T3 and T6). In the present case, the
31 absorption edge corresponds to the lowest energy transition in the T6 system, while
32 the excitation responsible of the spectral edge of the T3 system could be identified at
33 224.6 nm. Indeed, the orbitals involved in the UV-Vis transitions resemble the frontier
34 orbitals of the C_{tetra} clusters with Ti in T3 and T6. For instance, the HOMO is mainly
35
36
37
38
39
40
41
42
43
44
45
46
47
48
49
50
51
52
53
54
55
56
57
58
59
60

1
2
3
4
5 localized on the 2p oxygens around Ti in T6, while the HOMO-1 is spread over all
6
7 oxygens of the 5-ring. All of the lowest unoccupied MOs have Ti-3d character: In
8
9 particular, the LUMO and LUMO+1 are mainly related to Ti d-states in T6 with a
10
11 minor contribution of Ti-d in T3, while LUMO+2 is predominantly localized on T3
12
13 and slightly contaminated by Ti-d in T6. Therefore, a small degree of mixing between
14
15 Ti d states is present, thus allowing partial delocalization of the lowest unoccupied
16
17 MOs on nearest-neighboring Ti centers.
18

19
20 On the other hand, direct interaction between Ti centers like in the Ti-O-Ti bridge
21
22 ($\text{Ti}^1\text{-Ti}^2=3.495 \text{ \AA}$, with Ti^1 in T3 and Ti^2 in T4) leads to a large red shift of the UV-
23
24 Vis edge (to 248 nm), as well as to significant modifications in the absorption profiles
25
26 (Figure 11). Such a pronounced change arises from drastic alterations in the TS-1
27
28 electronic structure. In particular, the lowest unoccupied states could no longer be
29
30 described as Ti d states in a tetrahedral CFT, because the TiO_4 units forming the Ti-
31
32 O-Ti moiety do share an oxygen atom and are, therefore, bonded to each other. This
33
34 allows d-orbital mixing between Ti centers, with relevant consequences on both elec-
35
36 tronic excitation and bonding properties. Concerning the latter, electronic structure
37
38 analysis highlighted that several low-energy MOs (not involved in optical transitions)
39
40 delocalized on the Ti-O-Ti moiety contain a major contribution of Ti d states and are
41
42 characterized by a pronounced bonding character in the Ti-O-Ti region (Figure 12).
43
44 Such a large Ti-d participation in bonding is responsible of a particularly strong Ti-O-
45
46 Ti interaction and explains why the Ti-O bond distances in the bridge are the shortest
47
48 ones (see Table 3). However, d-d mixing not only stabilizes the bonding states, but its
49
50 effect is even greater on the lowest unoccupied MOs, the LUMO and LUMO+1, which
51
52 correspond to the arrival states of the lowest-energy electronic transitions: As a result,
53
54 the edge of the excitation spectrum is redshifted.
55

56
57 Actually, from detailed assignment of the spectral bands it emerges that all absorp-
58
59 tions beyond 205 nm involve excitations to the LUMO and LUMO+1 orbitals. The
60

1
2
3
4
5 absorption edge is due to the HOMO→LUMO transition, with the HOMO showing a
6 pure non-bonding O 2p character like in the case of low Ti-content systems. However,
7 the maximum peak (at 225 nm) is due to excitations starting from $b-t_{2g}^{(O)}$ -like states
8 where the extent of Ti-d contamination is higher than in the isolated Ti centres cases.
9 Also at smaller wavelengths, the bands could be generally ascribed to excitations from
10 delocalized O 2p states with smaller Ti-d character, to low energy empty states de-
11 riving from the combination of the empty d-orbitals. Interestingly, such excited states
12 (Figure 12b,c) are spread over the Ti-O-Ti moiety and evenly localized on both Ti
13 centres. Therefore, d-d mixing also causes excited electrons to be more delocalized
14 with respect to the case of an isolated Ti centre.
15
16
17
18
19
20
21
22
23
24
25

26 4 Summary and conclusions

27
28
29
30 Non-defective TS-1 models have been investigated by means of periodic DFT calcu-
31 lations, with the aim of contributing to the issue of Ti preferential positioning. The
32 molecular complexity underlying the TS-1 synthesis process makes it difficult to single
33 out the factor that actually determines Ti preferential location in such a relevant ma-
34 terial.¹⁹ Nevertheless, from the results here presented, a non random Ti siting in TS-1
35 emerged on the basis of thermodynamics (energetics) considerations only.
36
37
38
39
40
41

42 For a Ti content corresponding to 1.35% in weight of TiO_2 (one Ti in 96 T sites) the
43 structures with titanium siting in T3 or T4 are the most probable.
44
45

46 The siting problem becomes more involved for higher Ti content, here analyzed in
47 a limited set of possible structures, corresponding to a Ti content of 2.70% in weight
48 of TiO_2 (i.e. 2 Ti over 96 T sites). In this case, both the kind of Ti sites and their
49 Ti-Ti separation play a relevant role for the relative stability.
50
51
52

53 Quite interestingly, the presence of a Ti-O-Ti bridge (Ti-Ti distance of 3.5 Å), where
54 both Ti are in a tetrahedral TiO_4 geometry, is not particularly destabilized with re-
55 spect to different double Ti substitutions. Actually one of such structures is only 2.7
56
57
58
59
60

1
2
3
4
5 kcal/mol higher in energy with respect to the most stable one in the sampled configura-
6
7 rations.
8

9 Starting from the optimized periodic structures, electronic excitation spectra were ob-
10 tained by adopting a cluster approach and a TD-DFT calculation scheme. All of the
11 different Ti sites present absorption profiles in the 200-230 nm UV region in line with
12 DRUV-Vis experiments on low Ti content dry TS-1 samples. The excitations present
13 a multiband profile which is characteristic of each different T site. The actual profiles
14 are strictly interlaced with distortion from the perfect tetrahedral symmetry which is
15 different for different crystallographic sites. The absorption bands involve transitions
16 from oxygen lone pairs to empty d-states localized on Ti (i.e. LMCT: ligand to metal
17 charge transfer transitions), in line with the current opinion.
18
19
20
21
22
23
24
25
26
27

28 Our results however suggest a description more complex than the standard picture,
29 based on $O^{2-} + Ti^{4+} \rightarrow O^{-} + Ti^{3+}$ transitions involving only Ti-bound oxygen atoms.
30 Actually, we propose that UV-Vis transitions in titanium zeolites would occur from
31 framework oxygens bands to localized Ti empty states. The participation of extended
32 electronic structures to the UV transitions in Ti zeolites may be a key point in explain-
33 ing the photoconducting properties recently highlighted in Ti zeolites (TS-1 included).³
34 Besides electronic excitations, analysis of the vibrational properties has been per-
35 formed. From the investigations on isolated Ti sites a picture in line with previous
36 analysis emerges: the 960 cm^{-1} band in the IR transparent silica window can be as-
37 sociated to tetrahedral Ti, along with a raman active feature detected at 1125 cm^{-1} .
38 Some interesting features however emerged from the vibrational spectra of Ti-O-Si-
39 O-Ti and Ti-O-Ti bridges. Associated to the first structure, we have found an IR
40 active band just in the center of the silica window, at 908 cm^{-1} , that could be easily
41 detectable in the experimental IR spectra. The absence of such a band in the available
42 IR spectra of TS-1 indicates that the presence of such a structure can be excluded in
43 real TS-1. More problematic could be the clear-cut exclusion of a Ti-O-Ti bridge: in-
44
45
46
47
48
49
50
51
52
53
54
55
56
57
58
59
60

1
2
3
4
5
6
7
8
9
10
11
12
13
14
15
16
17
18
19
20
21
22
23
24
25
26
27
28
29
30
31
32
33
34
35
36
37
38
39
40
41
42
43
44
45
46
47
48
49
50
51
52
53
54
55
56
57
58
59
60

deed this structure gives IR signatures (853 and 1003 cm^{-1}) which are just at the edge of the silica window. Also an intense raman active mode calculated at 1115 cm^{-1} can be compatible with the tetrahedral Ti "raman signature" at 1125 cm^{-1} . Moreover its calculated absorption edge at 248 nm is compatible with available TS-1 data. Probably such a (tetrahedral Ti) Ti-O-Ti structure could be considered a nucleation center for the (octahedral Ti) TiO_2 phase separation. Indeed, for the TiO_2 phase growth, which is known to occur at Ti contents higher than 2.5%, Ti-O-Ti bridges should be formed. Our results, which demonstrate the stability of this moiety in models of comparable Ti content, its compatibility with available spectroscopic data and its peculiar electronic properties, suggest therefore further experimental work aimed at the identification and characterization of Ti-O-Ti bridges in the TS-1 framework.

	ΔE	Ti-O	Ti-O	Ti-O	Ti-O	$\langle \text{Ti-O} \rangle$
T1	5.59	1.7855	1.7928	1.7955	1.7965	1.7926
T2	3.87	1.7912	1.7914	1.7971	1.7984	1.7945
T3	0.0	1.7827	1.7905	1.7931	1.8040	1.7925
T4	0.28	1.7895	1.7965	1.7971	1.7989	1.7955
T5	2.84	1.7935	1.8006	1.8013	1.8030	1.7996
T6	4.92	1.7919	1.7952	1.7959	1.8039	1.7967
T7	4.06	1.7881	1.7936	1.7962	1.8085	1.7966
T8	2.29	1.7778	1.7934	1.7959	1.8105	1.7944
T9	2.23	1.7803	1.7978	1.7987	1.8042	1.7953
T10	4.20	1.7923	1.7951	1.7969	1.8039	1.7971
T11	1.41	1.7929	1.7943	1.8041	1.8096	1.8002
T12	1.48	1.7867	1.7917	1.8023	1.8048	1.7964

Table 1: Calculated ΔE (in kcal/mol), optimized Ti-O bond distances and average $\langle \text{Ti-O} \rangle$ distances *vs.* T site. Distances in Å.

	<hr/>							<OTiO>	<hr/>
T1	108.7	113.3	111.0	107.5	108.6	107.6	109.4		
T2	108.2	107.8	110.3	107.5	112.5	110.4	109.4		
T3	109.9	108.0	110.5	107.3	109.5	111.6	109.5		
T4	110.3	105.6	112.0	108.3	109.7	110.9	109.5		
T5	110.5	106.6	108.8	109.9	108.6	112.3	109.5		
T6	109.0	109.8	109.4	110.8	106.9	110.9	109.5		
T7	108.1	108.5	109.9	108.2	112.2	109.7	109.5		
T8	109.0	108.6	106.9	111.5	108.7	112.0	109.4		
T9	110.0	109.4	110.1	106.1	110.5	110.6	109.5		
T10	109.4	110.3	109.6	108.3	109.7	109.5	109.5		
T11	107.4	108.8	110.9	108.6	110.6	110.4	109.5		
T12	108.7	109.3	112.0	110.1	109.4	107.2	109.5		

Table 2: Optimized O-Ti-O bond angles and average O-Ti-O bond angle (<OTiO>) *vs.* T site. Angles in degrees.

	Ti-Ti	Ti-O*	Ti-O	Ti-O	Ti-O	<Ti-O>
T3	3.4952	1.7761	1.7949	1.7978	1.8016	1.7918
T4	3.4952	1.7870	1.7934	1.7940	1.7976	1.7930

Table 3: Optimized Ti-Ti separation and Ti-O bond distances for a $[\text{Ti}_2\text{Si}_{94}\text{O}_{192}]$ structure characterized by Ti in T3 and T4 with a Ti-O-Ti bridge. The Ti-O* entry refers to the Ti-O-Ti bonds. Distances in Å.

	<OTiO>						
T3	106.1	108.1	108.3	109.6	111.8	112.6	109.4
T4	106.2	106.9	108.6	109.1	111.8	114.1	109.5

Table 4: Optimized O-Ti-O bond angles and average O-Ti-O bond angle (<OTiO>) for a $[\text{Ti}_2\text{Si}_{94}\text{O}_{192}]$ structure characterized by Ti in T3 and T4 with a Ti-O-Ti bridge. Angles in degrees.

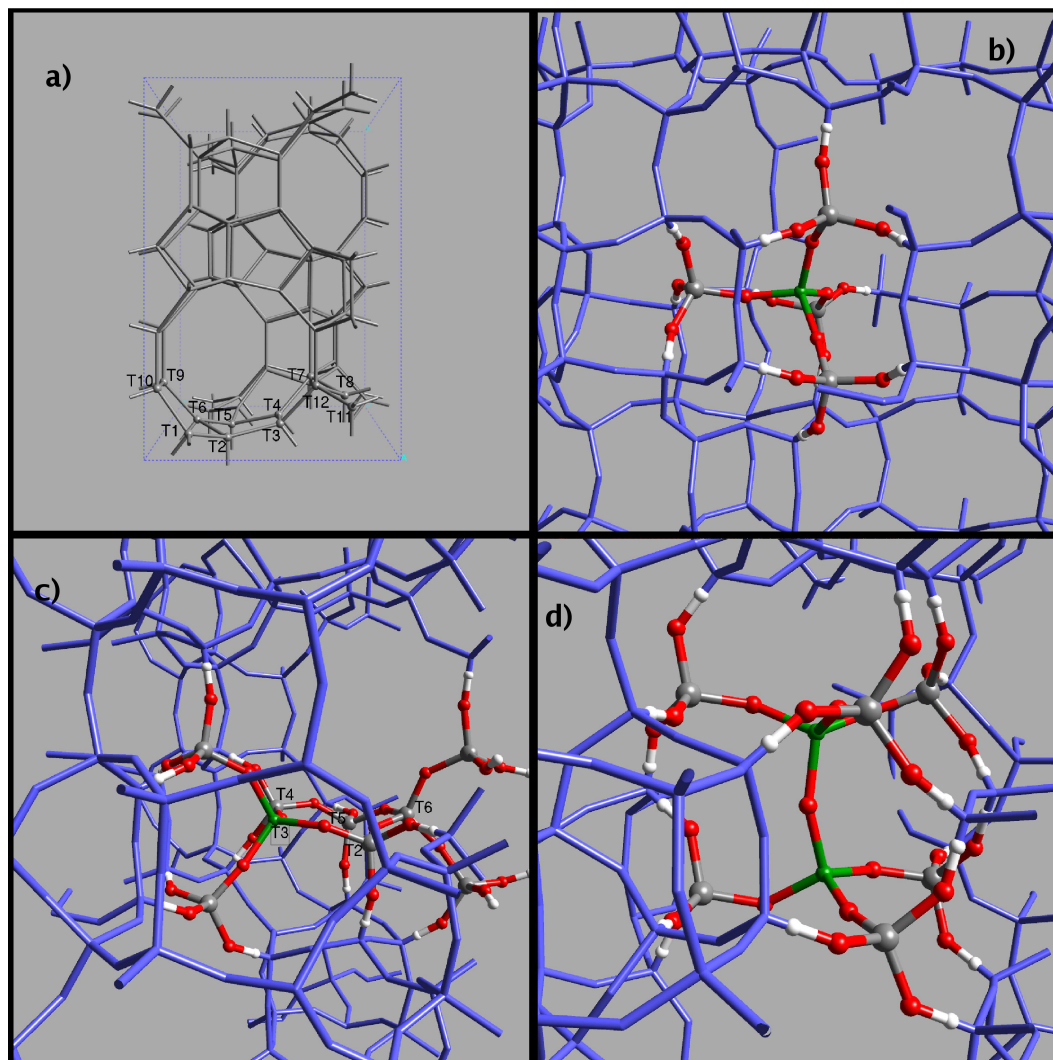


Figure 1: a) Graphical representation of the MFI unit cell. Only T atoms are represented. Also reported are the labels of the twelve independent T sites. b) Ball-and-stick Ti[O-(Si(OH)₃]₄ cluster (C_{tetra}) superimposed on the TS-1 crystal (blue sticks). Color codes: Si, gray spheres; O, red spheres; H, white spheres; Ti, green sphere. c) Ball-and-stick representation of a C_{5-ring} cluster superimposed on the TS-1 crystal (blue sticks). Color codes: Si, gray spheres; O, red spheres; H, white spheres; Ti, green sphere. d) Ball-and-stick representation of a Ti-O-Ti bridge structure (C_{2tetra} cluster) superimposed on the TS-1 crystal (blue sticks). Color codes: Si, gray spheres; O, red spheres; H, white spheres; Ti, green spheres.

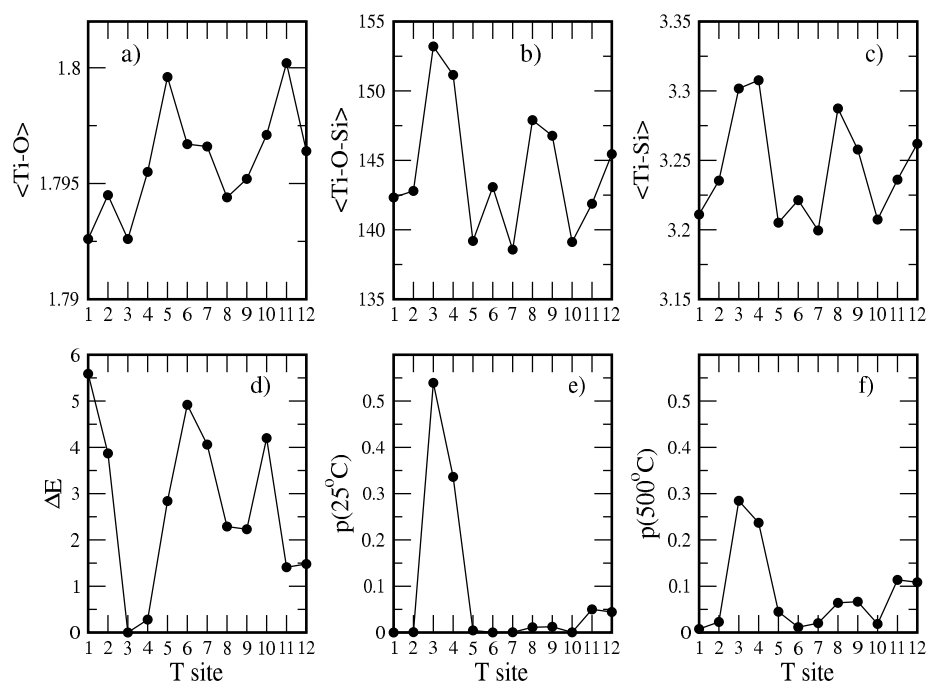


Figure 2: Selected properties of $[\text{TiSi}_{95}\text{O}_{192}]$ characterized by different siting of Ti. a): average Ti-O bond distances (in Å) for different Ti siting. b): average Ti-O-Si angles (in degrees) for different Ti siting. c): average Ti-Si separation (in Å) for different Ti siting. d): PBE/VDB/30 ΔE (in kcal/mol) calculated with respect to Ti in T3. e): normalized probability of occurrence of Ti in the 12 T sites at 25 °C. f): normalized probability of occurrence of Ti in the 12 T sites at 500 °C.

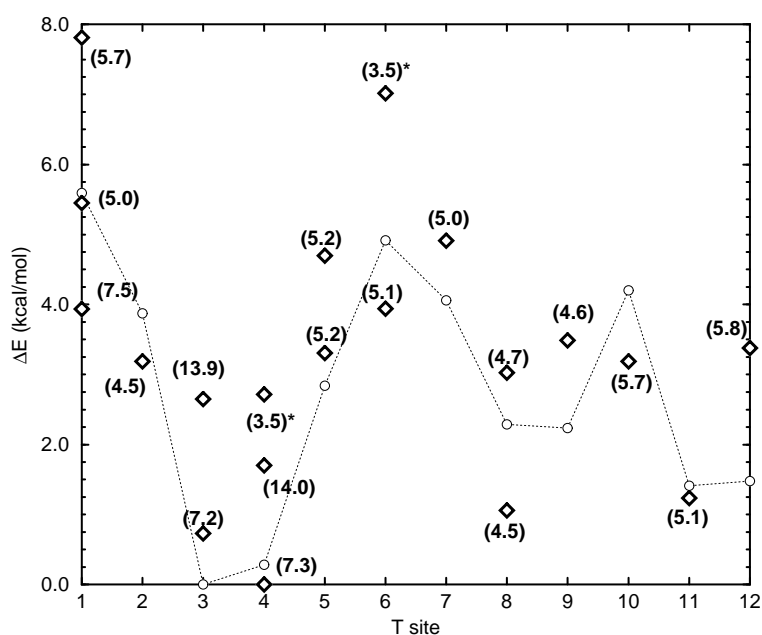


Figure 3: Energy differences ΔE in kcal/mol of selected $[\text{Ti}_2\text{Si}_{94}\text{O}_{192}]$ configurations. In all configurations, Ti^1 is positioned in T3. They differ by the siting of Ti^2 . The diamonds represent the energy relative to the most stable configuration among the sampled ones (Ti^1 in T3 and Ti^2 in T4), with the corresponding Ti^1 - Ti^2 distance (in Å) reported in parenthesis. Configurations labeled with a star are characterized by a Ti-O-Ti bridge. Circles connected by a dashed line represent the energy scale for a single Ti substitution ($[\text{TiSi}_{95}\text{O}_{192}]$).

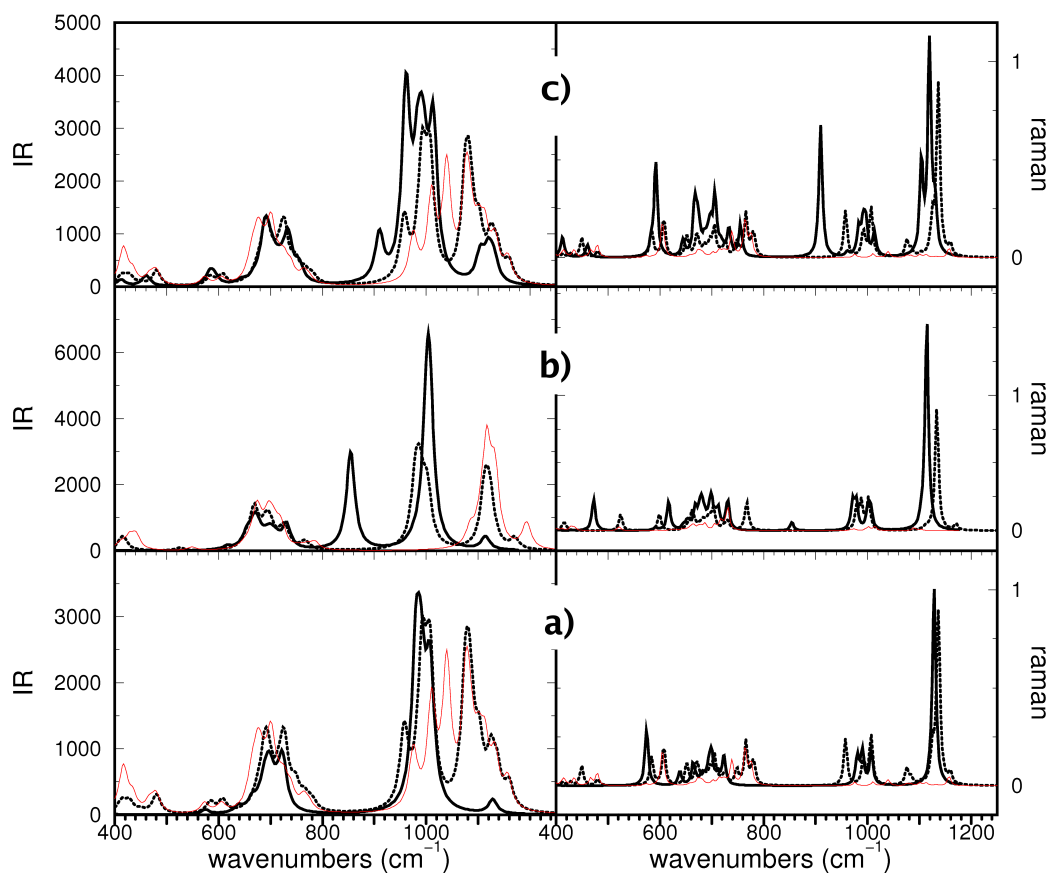


Figure 4:

Calculated IR (left panels) and raman (right panels) intensities. a) thick-line: C_{tetra} with Ti in T3; dashed-line: C_{5-ring} with Ti in T3; red-line: all silica C_{5-ring} . b) thick-line: C_{2tetra} with a Ti-O-Ti bridge, Ti in T3 and T4; dashed-line: C_{2tetra} with one Ti in T3; red-line: all silica C_{2tetra} . c) thick-line: C_{5-ring} with a Ti-O-Si-O-Ti bridge, Ti in T3 and T6; dashed-line: C_{5-ring} with one Ti in T6; red-line: all silica C_{5-ring} .

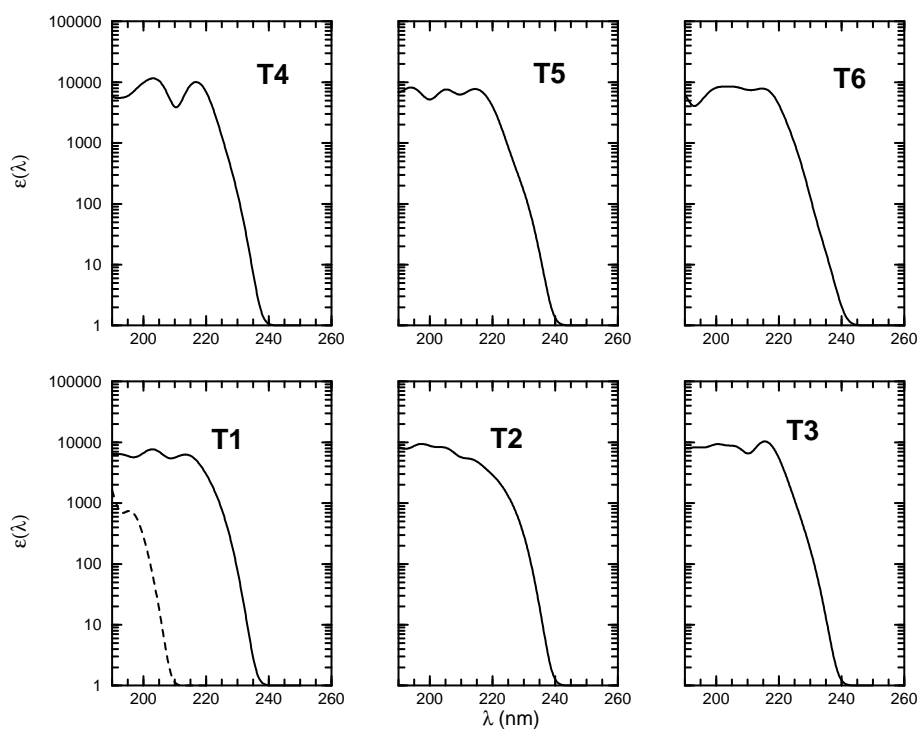


Figure 5: Calculated TD-DFT excitation spectra of cluster models cut from $[Ti_1Si_{95}O_{192}]$ DFT optimized structures. Calculated spectra are relative to C_{tetra} with Ti in the T1, T2, T3, T4, T5 and T6 sites. The excitation spectrum for a C_{tetra} all silica cluster (site T1) is reported for comparison (dashed line).

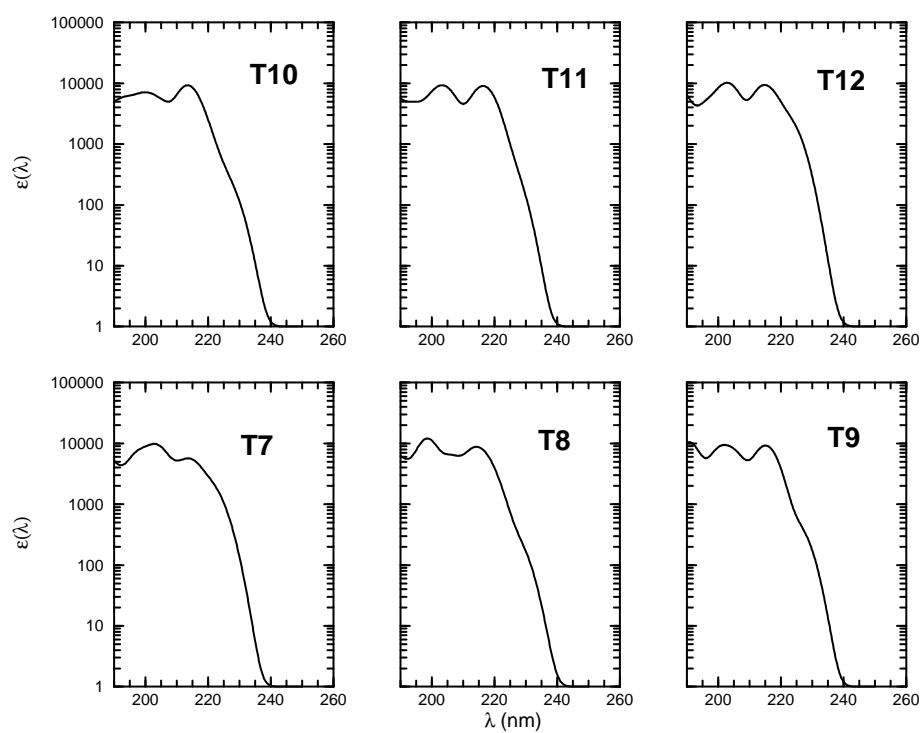


Figure 6: Calculated TD-DFT excitation spectra of cluster models cut from $[\text{Ti}_1\text{Si}_{95}\text{O}_{192}]$ DFT optimized structures. Calculated spectra are relative to C_{tetra} with Ti in the T7, T8, T9, T10, T11 and T12 sites.

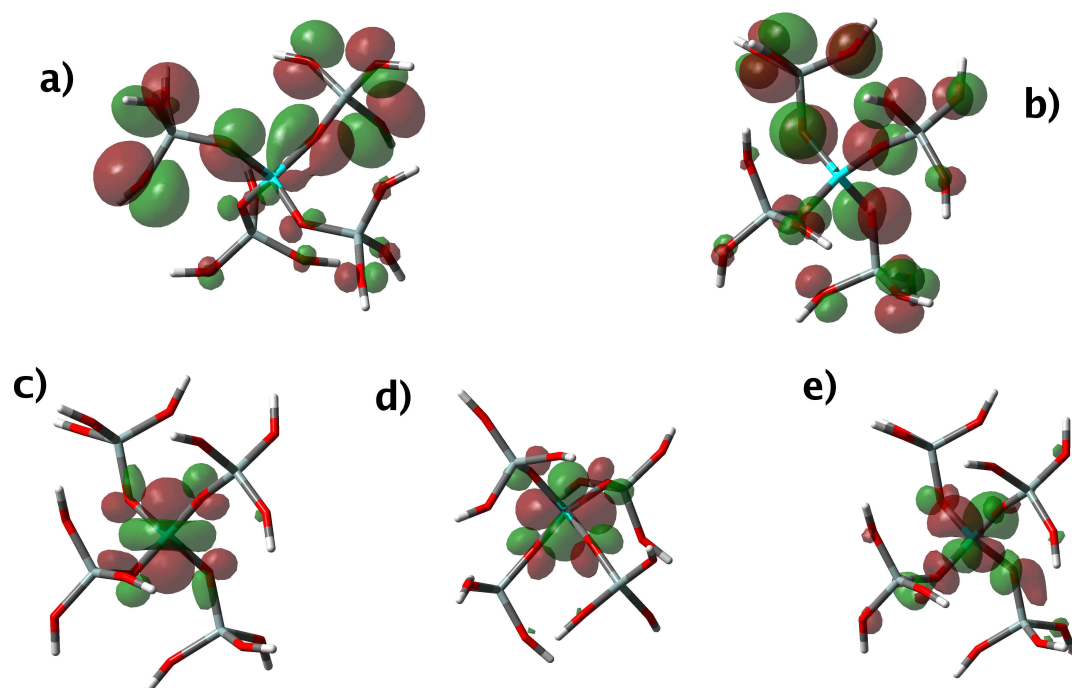


Figure 7: Representative examples of frontier molecular orbitals involved in electronic transitions in one C_{tetra} ($Ti-(O-Si(OH)_3)_4$) cluster, Ti in T6. a) $b-t_{2g}^{(O)}$ occupied orbital; b) $nb-t_{2g}^{(O)}$ occupied orbital; c) $e_g^{(E)}$ unoccupied orbital; d) $e_g^{(E)}$ unoccupied orbital; e) $t_{2g}^{(E)}$ unoccupied orbital. Green and red contours represent positive and negative orbital lobes. Atoms color codes: Ti, cyan; Si, gray; O, red; H, white.

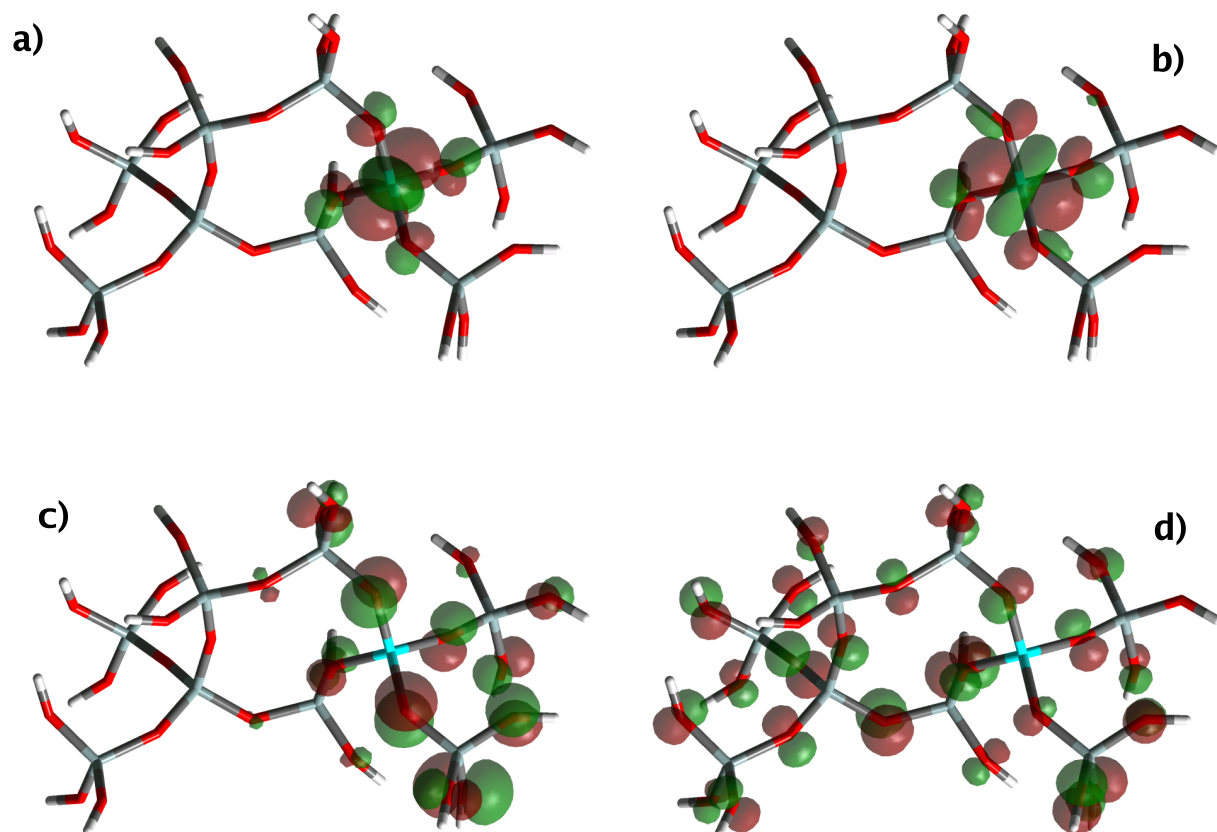


Figure 8: Representative examples of frontier molecular orbitals involved in electronic transitions for a C_5 -ring structure with one Ti (in T6). a) $e_g^{(E)}$ unoccupied orbital; b) $e_g^{(E)}$ unoccupied orbital. c) $nb-t_{2g}^{(O)}$ occupied orbital (HOMO); d) $nb-t_{2g}^{(O)}$ occupied orbital. Color codes as in Figure 7.

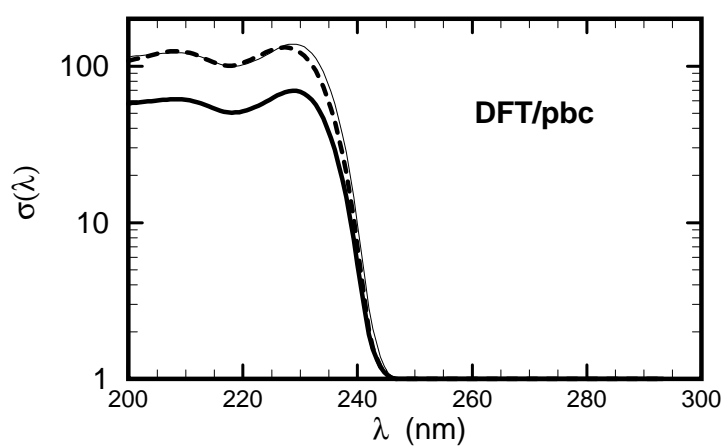


Figure 9: DFT optical conductivity σ calculated for crystal structures (with pbc). Thick line: $[\text{Ti}_1\text{Si}_{95}\text{O}_{192}]$ structure with one Ti in T3; thick-dashed line: $[\text{Ti}_2\text{Si}_{94}\text{O}_{192}]$ structure with Ti in two well separated T3 sites (Ti-Ti distance = 14.0 Å) Thin line: twice the optical conductivity σ calculated for the $[\text{Ti}_1\text{Si}_{95}\text{O}_{192}]$ structure with one Ti in T3.

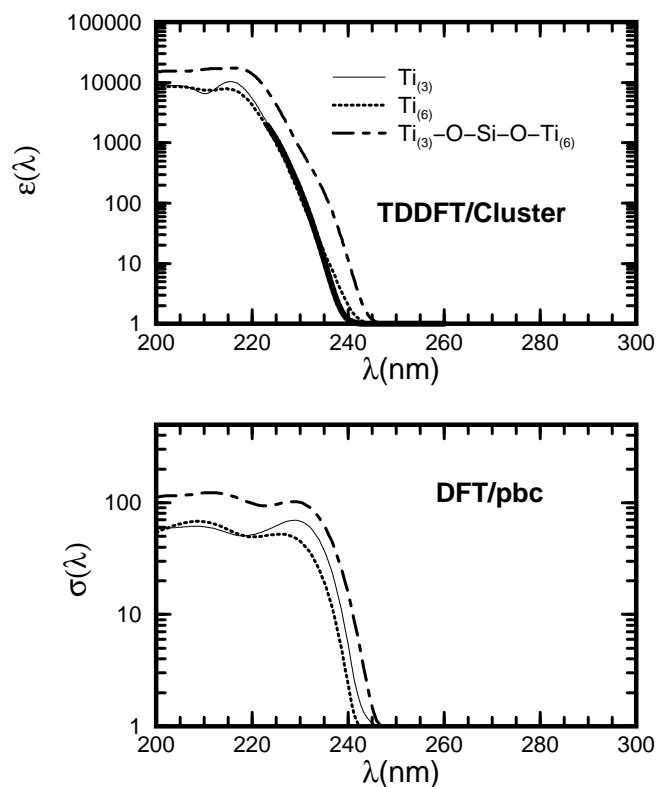


Figure 10: Top: TD-DFT absorbance spectra calculated for cluster models. Thin-line: C_{tetra} cluster with Ti in T3; thick-dotted-line: C_{tetra} cluster with Ti in T6; thick-dot-dashed line C_{5-ring} with a Ti-O-Si-O-Ti bridge, Ti in T3 and T6 cut from $[\text{Ti}_2\text{Si}_{94}\text{O}_{192}]$ Bottom: DFT optical conductivity σ calculated for crystal structures (with pbc). Thin black line: $[\text{TiSi}_{95}\text{O}_{192}]$ with Ti in T3; thick-dashed line: $[\text{TiSi}_{95}\text{O}_{192}]$ with Ti in T6; thick-dot-dashed line: $[\text{Ti}_2\text{Si}_{94}\text{O}_{192}]$ system with Ti^1 in T3 and Ti^2 in T6.

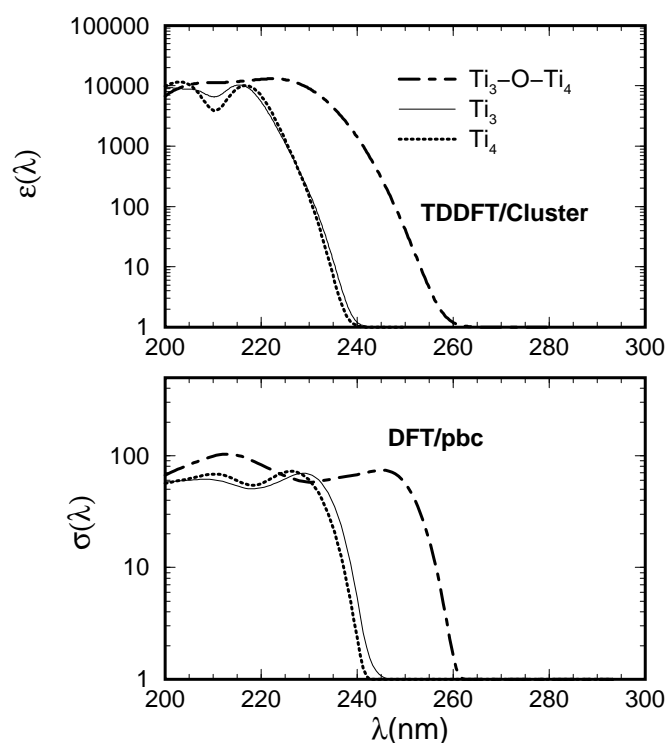


Figure 11: Top: TD-DFT absorbance spectra calculated for cluster models cut from $[Ti_1Si_{95}O_{192}]$ with Ti in T3 (thin line) and T4 (thick dotted line) and from a $[Ti_2Si_{94}O_{192}]$ with Ti both in T3 and T4 corresponding to a Ti-O-Ti structure. Bottom: DFT optical conductivity calculated for the crystal structures (with pbc). Thin black line: one Ti in T3; thick-dashed line: one Ti in T4; thick-dot-dashed line: double Ti substitution in both T3 and T4.

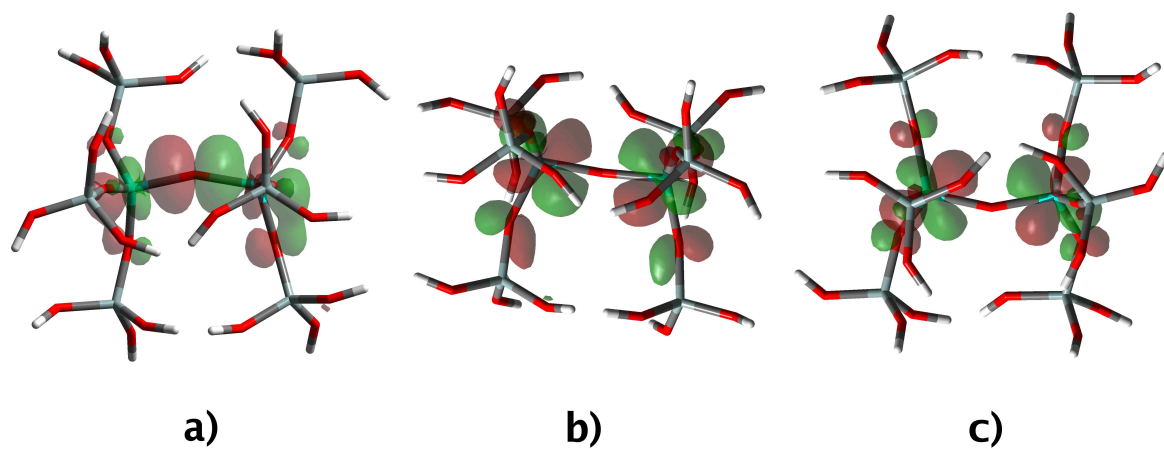


Figure 12: Relevant molecular orbitals in a cluster model containing a Ti-O-Ti bridge. a) bonding MO with dominant d_{z^2} character; b) LUMO, formed by combination of Ti-d states from both Ti centers; c) LUMO+1, formed by combination of Ti-d states from both Ti centers. Color codes as in Figure 7.

References

1. Clerici, M. G.; Bellussi, G.; Romano, U. *J. Catal.* **1991**, *129*, 159.
2. Taramasso, M.; Perego, G.; Notari, B. *US Patent 441051* **1983**, .
3. Atienzar, P.; Valencia, S.; Corma, A.; Garcia, H. *ChemPhysChem* **2007**, *8*, 1115.
4. Baerlocher, C.; Meier, W. M.; Olson, D. H. *Atlas of Zeolite Framework Types*; Elsevier: The Netherlands, 2001.
5. van Kóningsveld, H.; van Bekkum, H.; Jansen, J. C. *Acta Crystallogr. B* **1987**, *43*, 127.
6. Millini, R.; Perego, G.; Berti, D.; Parker, W. O.; Carati, A.; Bellussi, G. *Micropor. Mesopor. Mater.* **2000**, *35-36*, 387.
7. Millini, R.; Previdi Massara, E.; Perego, G.; Bellussi, G. *J. Catal* **1992**, *137*, 497.
8. Scarano, D.; Zecchina, A.; Bordiga, S.; Geobaldo, F.; Spoto, G.; Petrini, G.; Leofanti, G.; Padovan, M.; Tozzola, G. *J. Chem. Soc. FARADY TRANS.* **1993**, *89*, 4123.
9. Li, C.; Xiong, G.; Xin, Q.; Liu, J.; Ying, P.; Feng, Z.; Li, J.; Yang, W.; Wang, Y.; Wang, G.; Liu, X.; Lin, M.; Wang, X.; Min, E. *Angew. Chem. Int. Ed.* **1999**, *38*, 2320.
10. Le Noc, L.; Trong On, D.; Solomykina, S.; Echchahed, B.; Beland, F.; Cartier Dit Moulin, C.; Bonneviot, L. *Stud. Surf. Sci. Catal.* **1996**, *101*, 611.
11. Lamberti, C.; Bordiga, S.; Arduino, D.; Zecchina, A.; Geobaldo, F.; Spanó, G.; Genoni, F.; Petrini, G.; Carati, A.; Villain, F.; Vlaic, G. *J. Phys. Chem. B* **1998**, *102*, 6382.

- 1
2
3
4
5
6 12. Lamberti, C.; Bordiga, S.; Zecchina, A.; Artioli, G.; Marra, G.; Spanó, G. *J.*
7 *Am. Chem. Soc.* **2001**, *123*, 2204.
8
9
10 13. Hijar, C. A.; Jacubinas, R. M.; Eckert, J.; Henson, N. J.; Hay, P. J.; Ott, K. C.
11 *J. Phys. Chem. B* **2000**, *104*, 12157.
12
13
14 14. Henry, P. F.; Weller, M. T.; Wilson, C. C. *J. Phys. Chem. B* **2001**, *105*, 7452.
15
16
17 15. Deka, R. C.; Nasluzov, V. A.; Ivanova Shor, E. A.; Shor, A. M.; Vayssilov, G. N.;
18 Rösch, N. *J. Phys. Chem. B* **2005**, *109*, 24304.
19
20
21 16. Ricchiardi, G.; de Man, A. J. M.; Sauer, J. *Phys. Chem. Chem. Phys.* **2000**, *2*,
22 2195.
23
24
25 17. Sastre, G.; Corma, A. *Chem. Phys. Lett.* **1999**, *302*, 447.
26
27
28 18. Millini, R.; Perego, G.; Seiti, K. *Stud. Surf. Sci. Catal.* **1994**, *84*, 2123.
29
30
31 19. Parker, W. O.; Millini, R. *J. Am. Chem. Soc.* **2006**, *128*, 1450.
32
33
34 20. Boccuti, M. R.; Rao, K. M.; Zecchina, A.; Leofanti, A.; Petrini, G. *Stud. Surf.*
35 *Sci. Catal.* **1988**, *48*, 133.
36
37
38 21. Perdew, J. P.; Burke, K.; Ernzerhof, M. *Phys. Rev. Lett.* **1996**, *77*, 3865-3868.
39
40
41 22. Vanderbilt, D. *Phys. Rev. B* **1990**, *41*, 7892.
42
43
44 23. He, Y.; Tilocca, A.; Dulub, O.; Selloni, A.; Diebold, U. *Nature Mat.* **2009**, *8*,
45 585.
46
47
48 24. Tilocca, A.; Fois, E. *J. Phys. Chem. C* **2009**, *113*, 8683.
49
50
51 25. Trudu, F.; Tabacchi, G.; Gamba, A.; Fois, E. *J. Phys. Chem. A* **2007**, *111*,
52 11626.
53
54
55
56
57
58
59
60

- 1
2
3
4
5 26. Trudu, F.; Tabacchi, G.; Gamba, A.; Fois, E. *J. Phys. Chem. C* **2008**, *112*,
6 15394.
7
8
9
10 27. *CPMD code*; (www.cpmid.org): Copyright MPI für Festkörperforschung, Stuttgart,
11 and IBM Zürich Research Laboratory, 1990-2006.
12
13
14
15 28. Runge, E.; Gross, E. K. *Phys. Rev. Lett.* **1984**, *52*, 997.
16
17
18 29. Casida, M. E.; Jamorsky, C.; Casida, K. C.; Salahub, D. R. *J. Chem. Phys.*
19 **1998**, *108*, 4439.
20
21
22
23 30. Becke, A. D. *J. Chem. Phys.* **1993**, *98*, 5648.
24
25
26 31. Frisch, M. J. *et al. Gaussian 03, Revision D.02*; Gaussian, Inc.: Wallingford CT,
27 2004.
28
29
30
31 32. Kleinman, L.; Bylander, D. M. *Phys.Rev.Lett* **1982**, *48*, 1425.
32
33
34 33. Troullier, N.; Martins, J. L. *Phys.Rev. B* **1991**, *43*, 1993.
35
36
37 34. Spanó, E.; Tabacchi, G.; Gamba, A.; Fois, E. *J. Phys. Chem. B* **2006**, *110*,
38 21651-21661.
39
40
41 35. Fois, E.; Gamba, A.; Tabacchi, G. *ChemPhysChem* **2005**, *6*, 1237.
42
43
44 36. Fois, E.; Gamba, A.; Tabacchi, G. *ChemPhysChem* **2008**, *9*, 538.
45
46
47 37. Scott, A. P.; Radom, L. *J. Phys. Chem.* **1996**, *100*, 16502.
48
49
50 38. Ricchiardi, G.; Damin, A.; Bordiga, S.; Lamberti, C.; Spano', G.; Rivetti, F.;
51 Zecchina, A. *J. Am. Chem. Soc.* **2001**, *123*, 11409.
52
53
54
55 39. Bordiga, S.; Coluccia, S.; Lamberti, C.; Marchese, L.; Zecchina, A.;
56 Boscherini, F.; Buffa, F.; Genoni, F.; Leofanti, G.; Petrini, G.; Vlaic, G. *J.*
57 *Phys. Chem.* **1994**, *98*, 4125.
58
59
60

- 1
2
3
4
5 40. Fan, W.; Duan, R.-G.; Yokoi, T.; Wu, P.; Kubota, Y.; Tatsumi, T. *J. Am.*
6 *Chem. Soc.* **2008**, *130*, 10150.
7
8
9
10
11
12
13
14
15
16
17
18
19
20
21
22
23
24
25
26
27
28
29
30
31
32
33
34
35
36
37
38
39
40
41
42
43
44
45
46
47
48
49
50
51
52
53
54
55
56
57
58
59
60